Composites Science and Technology 201 (2021) 108480

Contents lists available at ScienceDirect

Composites Science and Technology

journal homepage: http://www.elsevier.com/locate/compscitech

2D electrical resistance (ER) mapping to Detect damage for carbon fiber reinforced polyamide composites under tensile and flexure loading

Jong-Hyun Kim [a,b], Pyeong-Su Shin [a,b], Dong-Jun Kwon [b,**], Joung-Man Park [a,b,c,*]

[a] Department of Materials Engineering and Convergence Technology, Gyeongsang National University, Jinju, Republic of Korea
[b] Research Institute for Green Energy Convergence Technology (RIGET), Gyeongsang National University, Jinju, Republic of Korea
[c] Department of Mechanical Engineering, The University of Utah, Salt Lake City, UT, 84112, USA

ARTICLE INFO

Keywords:
Damage sensing
Interface
Micro-mechanics
Thermoplastic composites

ABSTRACT

The carbon fiber reinforced thermoplastic composites (CFRTC) has been applied in the manufacture of automobiles. The in-situ damage sensing and nondestructive evaluation techniques are important in automobile industries. In this paper, the damage of Carbon fiber (CF)/Polyamide (PA) composite was sensed in-situ using electrical resistance (ER) on tensile and flexural stresses in specimens. The CF dispersion in CF/PA composite was evaluated using ER and calculated using an empirical formula. The CF/PA composite was manufactured with different CF weight fractions using an injection process. The load on specimens was sensed using the difference of ER as the tensile and flexural loads increased. The correlation between load and difference of ER was arranged using some equations. The CF array form was evaluated using ER at 1 cell area of the CF/PA composite. The sensing ability in the CF/PA composite was dependent on the weight fraction of CF because of bad dispersion of CF. The CF dispersion and damage sensing of real-products made of CF/PA composite can be evaluated using ER. The 20 wt% CF added PA composite was the optimal condition for evaluation of dispersion of CF and damage sensing using ER.

1. Introduction

In various industries, composites had been used to parts and structures including the automotive industry. Important features for a successful composite manufacturing process for automobile should include high productivity (short cycle time for manufacturing), sustainability (recyclable), and inexpensive source materials. A long fiber reinforced thermoplastic (LFT) process was considered suitable for manufacturing composite automobile parts because it appears to satisfy these conditions [1–3]. The LFT process can be used with various source materials such as general thermoplastic polymers (polypropylene, PP) [4,5], engineering plastics (polyamide, PA, polycarbonate, PC) [6–9], and super-engineering plastics (polyphenylene sulfide, polyphthalamide, polyetheretherketone, etc.) [10–13].

In injection molding processes, the polymer matrix has a significant effect on the mechanical properties of fiber reinforced thermoplastic composites. It can be because the fiber length and fiber contents were limited to manufacture fiber reinforced thermoplastic composites [14,15]. In general, 30 wt% CF/PA composites were used to produce 250 MPa tensile strength high-performance parts. The PP was mixed to control interfacial properties between fiber and matrix, viscosity of molten composite type the reasonable cost of the products [16,17]. In current, long fiber was altered to fiber mat in current to decrease manufacturing time of products and it was said fiber mat thermoplastic process. This process had some critical problems that impregnation of polymer matrix was poor and the product of complex shape was not well manufactured [18,19]. CF was used as reinforcement for high-performance, however, CF containing in LFT pellet was limited to 20 wt% because CF had higher cost than glass fiber (GF). GF was used generally for reinforcement to decrease cost of product and, in current, hybrid pellet using GF and CF for LFT was used to decrease cost and maintain performance [20,21].

The mechanical properties and their standard deviations of these composite materials were affected by the interface between fiber and matrix and fiber dispersion in the composite. The evaluation of the quality of automobile parts was important and this technique was in the limelight. The damage area and the fiber array in composites were evaluated using x-ray computed tomography (CT) and ultrasonic testing

* Corresponding author. Department of Materials Engineering and Convergence Technology, Gyeongsang National University, Jinju, Republic of Korea.
** Corresponding author. Research Institute for Green Energy Convergence Technology (RIGET), Gyeongsang National University, Jinju, Republic of Korea.
E-mail addresses: rorrir@empas.com (D.-J. Kwon), jmpark@gnu.ac.kr (J.-M. Park).

https://doi.org/10.1016/j.compscitech.2020.108480
Received 30 June 2020; Received in revised form 28 August 2020; Accepted 23 September 2020
Available online 29 September 2020

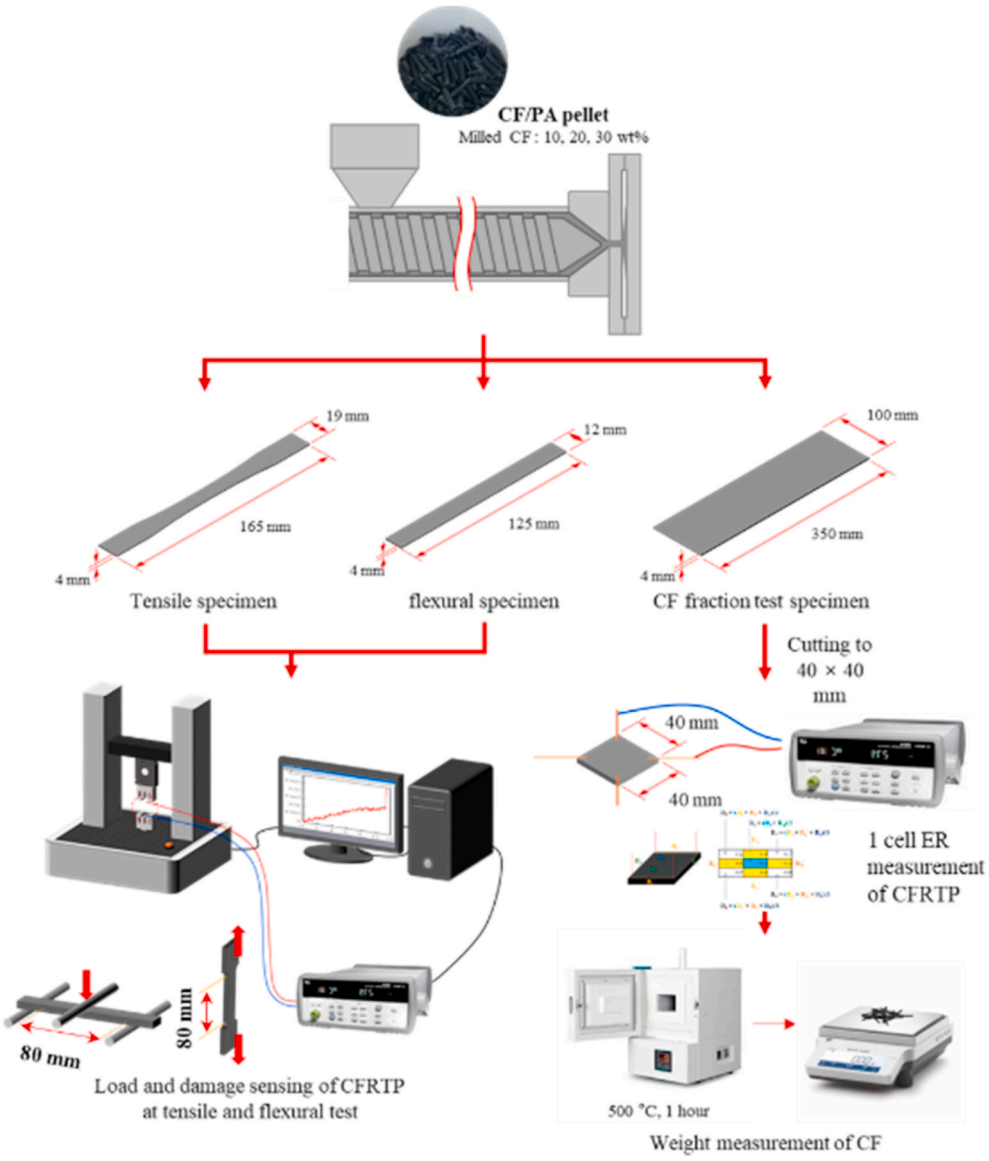

Fig. 1. Schematic plot for preparation process of the CF/PA composites.

(UT) [22,23]. Acoustic emission was used to sense damage the composites products. These damage sensing techniques have been studied in a number of automobile applications. J.M. Park and D.J. Kwon et al. have studied damage sensing *in-situ* by ER measurements in automobile parts via ER measurement tensile and flexural [16]. The studies of nondestructive evaluation (NDE) techniques of composite materials are indispensable while ceramic and metal materials have been studied from for a long time.

In this study, damage sensing and short fiber distribution in CF/PA composites for automobile parts were evaluated via ER measurement. The tensile and flexural stresses were applied to CF/PA composites using a universal testing machine (UTM) while ER measurements were made. ER measurements on the CF/PA composites specimens with different CF weight fractions. Empirical equations between CF contents and differences of ER were also established. CF dispersion of CF/PA specimens, that was made by injection molding, were evaluated via ER measurement. Finally, ER of real automotive products was measured to sense damage in the composite *in-situ*.

2. Experimental

2.1. Materials

CFRTC specimens were manufactured using 10, 20, 30 wt% CF (T700SC, Toray Co., LTD., Japan) added to PA 66 pellets (Hyundai EP Co. Ltd., Korea) by injection molding. This pellet/CF material was blended to make granules in an injection-molding machine with a co-rotating intermeshing twin-screw extruder (Bau-Tech, Korea). This extruder has a screw diameter of 19 mm and a distance between screw axes of 18.4 mm with L/D ratio of 40. The screw speed was 150 rpm, and the residence time for the melt was about 3 min. The samples for the mechanical testing were injected at a temperature profile with the steps of 200, 220, 240, and 260 °C.

2.2. ER measurement of CF/PA composite with tensile and flexural load

Fig. 1 shows the schematic arrangement of the preparation process for the CF/PA composite specimens. Tensile and flexural test specimens were manufactured with different CF weight fractions of CF/PA pellets by injection molding. Tensile test specimens were manufactured with

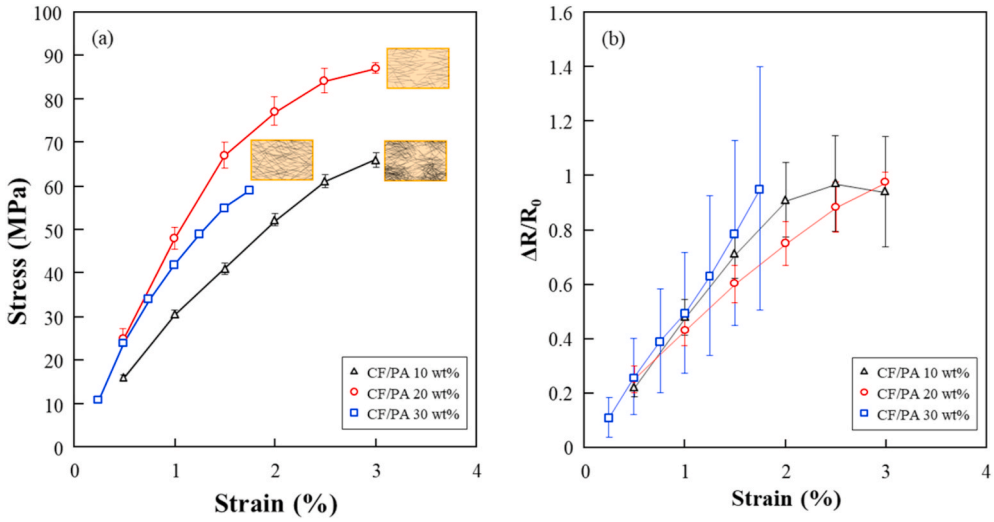

Fig. 2. (a) Stress-strain curves; and (b) ER change measurements during tensile testing of CF/PA with different CF contents.

165 mm in length, 19 mm in width, and in 4 mm thickness based on ASTM D638 and flexural test specimens were manufactured with 125 mm length, 12 mm width, and 4 mm thickness. Tensile and flexural tests were performed using a universal testing machine (UTM) (LR-10K, Lloyd, U.K.) at a strain rate of 10 mm/min. In this test, the contact point between the copper wire and CF/PA specimen was important to reduce ER noise and decrease error. In the tensile test specimens, the Cu wires were impregnated at a 100 mm gap between two Cu wires to not touch the area of the jig. In the flexural test specimens, the Cu wires were impregnated 5 mm from supports of jig to not touch the jig. All of ER measurements were performed by the 4-point probe ER measurement method for data acquisition (34927A, Agilent Technologies, Inc., U.S. A.). The fracture surfaces of the specimens were observed using a USB digital microscope (AM4515, AnMo Electronics Co., Taiwan) to observe the fiber aggregation area.

2.3. CF containing amount of CF/PA composite via ER measurement

The fiber content of the CF/PA composites was evaluated using 1 cell ER measurement [16]. Totally, 9 excel points were filled in ER data for 1 cell arranged ER data. ER 2D mapping results were possibly to combine several cell data using surface type graph by commercial excel program. Fiber containing specimens were manufactured with 350 mm in length, 100 mm in width, and 4 mm in thickness. From these 70 specimens were cut (40 mm in length and 40 mm in width) and the initial ER was measured by 1 cell probe ER measurement. Specimens were degraded in 500 °C at 1 h using a muffle furnace (MF-12HF, Jeio Tech, Korea) to remove PA and determine the amount (weight) of CF in the composite. An empirical equation between the initial ER and the amount of CF it contained was established.

The stability of the mechanical properties and dispersion of the CF in automobile parts made using 20 wt% CF PA composite were determined using 1 cell probe ER measurement. While real-specimen have complex forms, the specimens used in this study were in plate form (400 mm in length, 120 mm in width, and 3 mm in thickness). The ER of the specimens was measured at the initial state and in a heated state at 80 °C for 1 h. ER difference was calculated from the difference between the initial and heated ER states. The first step of preparation of ER mapping specimen was to fix the 0.1 mm Cu wire to the CF/PA surface using Scotch tape. The next step was to make rectangular spaces on the surface of specimens adjacent to the Cu wire to subsequently be filled with silver paste. The ER measurement section was divided into total 30 cells to evaluate the damage detection of the ER of the component. Length of one cell was 40 mm and shape of cell was square. The 10 cells in the horizontal direction and 3 cells in the vertical direction were formed. Eight copper wire contact sections per cell were formed and total 240 contacts were formed on the part. 2D ER mapping was performed by 4-probe method. Finally, polyimide tape was attached to the 4 probe tightly. The ER data was visualized using a contour chart and this chart showed a 2D surface that connects a set of data points for the damage sensing for the CFRTC [24].

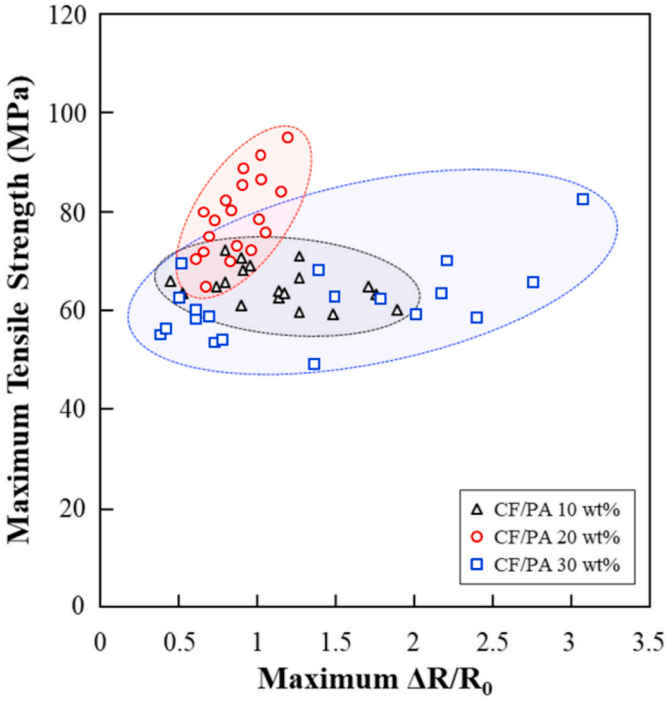

Fig. 3. Distribution trends between the ER difference and tensile strength of CF/PA composite with different CF weight fractions.

3. Results and discussion

3.1. Evaluation of tensile strength of CFRTC using ER sensing

Fig. 2(a) shows the tensile strength-strain curves for CF/PA composites with three different CF weight fractions, 10%, 20% and 30%. 20 wt% CF/PA composite had the largest tensile strength while the Young's

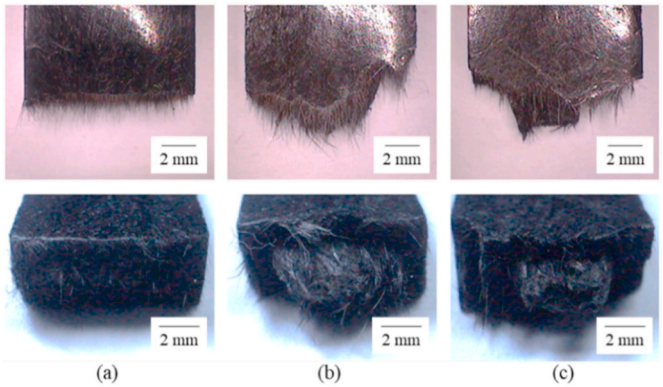

Fig. 4. Photograph of fracture surface after tensile testing of CF/PA composites with different CF weight fractions: (a) 10 wt%; (b) 20 wt%; and (c) 30 wt% CF/PA composites.

modulus as the slope of the curves tended to increase as the CF weight fraction increased up to 20%. Although the 30 wt% CF/PA composite was higher than other compositions in terms of initial tensile modulus, the overall optimum concentration was 20 wt% for maximized tensile strength, modulus and elongation of the CF/PA composites. It can be explained due to the CF dispersion state and further by Fig. 2(a). Inside schematic models describe the CF distribution in PA matrix with three different CF fractions.

Fig. 2(b) shows the ER difference *versus* tensile strain for the different CF weight fractions. ER difference of 20 wt% CF/PA composite was smallest, which means more uniform dispersion of CF in PA matrix. In standard difference (SD) of CF/PA composites, however, 30 wt% CF added CF/PA composite exhibited the largest ER difference in tensile load, which means less uniform of CF in PA matrix. The SD of ER of 10 wt % CF added CF/PA composite increased dynamically over 2% strain while the SD of ER of 10 wt% CF added CF/PA composite was the most stable under 2% strain. Both added conductive CFs and their dispersion can contribute to the final performance of CF/PA composites.

Fig. 3 shows the statistical distribution between ER difference ($\Delta R/R_o$) and tensile strength with 3 different CF weight fractions. In 20 wt% CF/PA composite case, the ER difference and tensile strength was more proportional trend and gathered with less scattering than those of 10 and 30 wt% CF/PA composites. In case 20 wt% CF/PA composite, the better proportional ER difference, the higher tensile strength. The 20 wt % CF could be optimized reasonably well via statistical distribution of

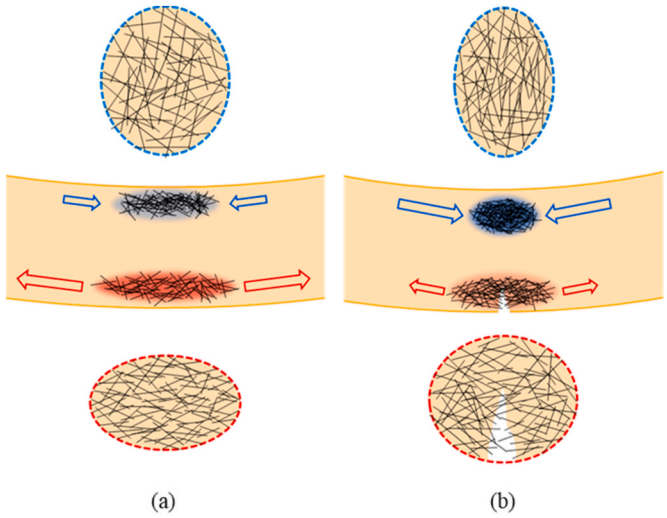

Fig. 6. Schematic plot of the flexural fracture process of CF/PA composites: (a) tension at lower part; (b) micro cracking of PA and breakage of some CFs at lower part.

ER difference. In case of 20 wt% CF/PA composite, the load of specimen was predicted from linear relationship between tensile strength and ER difference. In case of 10 and 30 wt% CF/PA composites, however, the distribution of ER was too broad not to predict the load of specimen. CF distribution. Their quality control in CF/PA composites can be also evaluated by standard deviation (SD) of ER measurements statistically.

Fig. 4 shows fracture surfaces for the CF/PA composites with different directions for 3 different CF weight fractions. Distinctly-different fracture patterns were observed as well. The dispersion of CFs in 20 wt% CF/PA composite was better than those with 10 and 30 wt % CF. In case of 10 wt% CF/PA composites, more uniformly-distributed CF tows were observed at the fractured surface. The more CF amounts, the more CF lump close to the center at fracture surface. With increasing CF amounts, non-uniformed distributed CF lumps resulted in various CF arrangements and thus non-uniform stress distributions. Initial fracture of CFRTC started to occur at poor CF region. Although CF distribution was relatively uniform in case 10 wt% CF/PA, CF contents in each region could be not equalized.

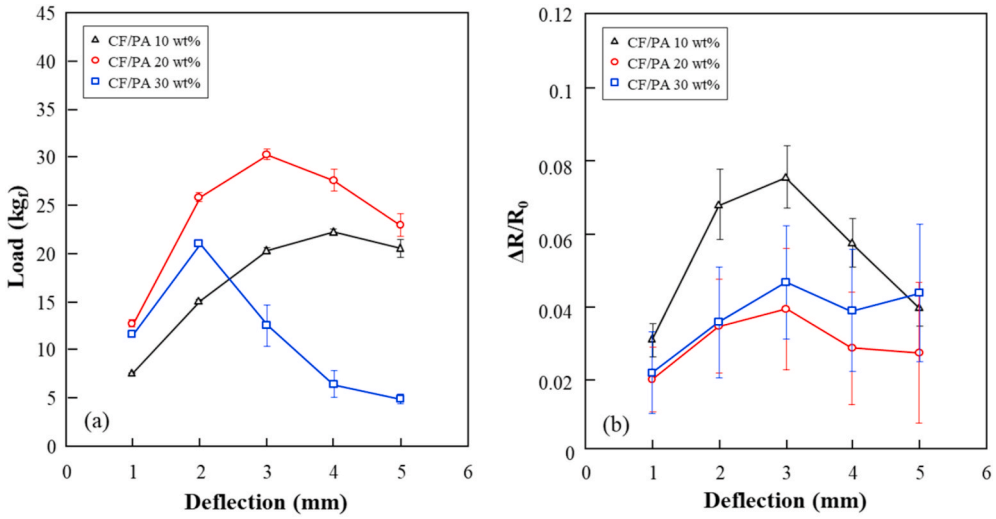

Fig. 5. Flexural loading and ER difference for different flexural deflections of CF/PA composites with different CF weight fractions: (a) flexural loading; and (b) ER difference.

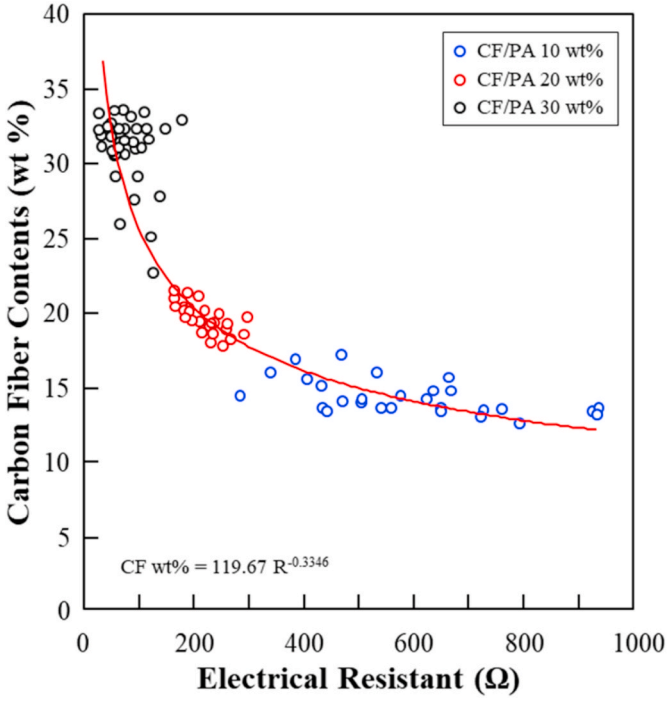

Fig. 7. CF contents *versus* ER of CF/PA composites and their trend fitting line.

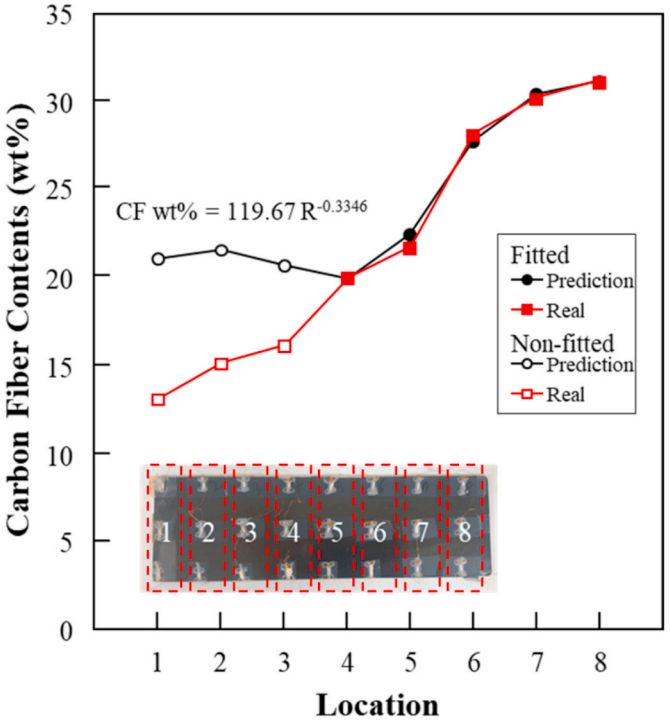

Fig. 8. Comparison between CF contents "predicted" using an empirical formula based on the trend fitting and "real" CF content and ER for each 8 section with actual experiments.

3.2. Evaluation of flexural strength of CFRTC using ER sensing

Flexural properties were measured along with the associated ER measurements while, in most prior researches tensile and compressive properties and their associated ER measurements have been studied [16,25,26]. Fig. 5 shows the flexural properties of CF/PA composites with different CF weight fractions using ER measurement.

In this work, the ER difference upon flexure loading was obtained with changing different CF weight fractions. Generally similar trend was that the maximum flexure strength was observed and the fracture in specimen occurred. In 20 wt% CF/PA case, the highest flexure strength was observed than those 10 wt% and 30 wt% cases although the curve trends were different from each other. Likewise, ER change exhibited opposite trends due to high conductivity in 20 wt case. Since dispersion of CF as well as CF contents were contribute to flexure strength and ER change together, those plots cannot be exactly same trends with 3 different CF contents. In 30% CF case, interlaminar fracture could occur at early deflection state, whereas ER did not decrease steeply correspondently due to still existing electrical connection.

Fig. 6 shows a schematic diagram of fracture steps for CF/PA composites in support of Fig. 5(a) and (b). In Fig. 6(a), tensile stresses are developed in the lower part of the specimen. The stress on the beam was sufficient to initiate a micro crack starting the specimen's fracture. In Fig. 6(b), a few CFs at the lower edge of the specimen resulted in a small increase in ER. However, the CFs in in the side of the specimen which under compression side of specimen are compacted in the PA matrix bringing them closer and in contact causing a decrease in ER. As the bending load increased, the fracture crack was driven completely through the sample by ever increasing tensile stress with a sudden dramatic increase in ER. Most of specimens fractured at over 5 mm deflection. For lower CF weight fractions flexural tests, the ER damage sensing measurements in the flexure of the CFRTC worked quite well and was informative. In case high CF weight fraction and thus the CF was not well dispersed, however, ER damage sensing was not effective.

3.3. Prediction of CF fraction and damage sensing in CFRTC using ER method

Fig. 7 shows the CF weight fractions *versus* ER. The ER of the CF/PA composite was measured and PA was thermal-degraded at 500 °C for 1.5 h. The ER increased as the CF weight fraction increased and the 20 wt% CF added PA composite had a narrower ER distribution trend line than others. For over 30 wt% CF addition, the distribution of ER was rather broader than for the others. The red line in was the trend fitting line using the data.

Fig. 8 shows the CF contents *versus* locations for a large specimen with 20 wt% GF comparing to the actual CF fractions. CF fractions were calculated using an empirical formula corresponding to the red fitting line in Fig. 7. The specimen was divided from 1 to 8 sections and their CF contents were measured in each sections. At front sections from 1 to 3, the calculated CF fraction were much lower than the real CF fractions. At back sections from 4 to 8, however, the calculated and the real CF fractions were similar each other. For these latter sections, the CF fraction could be accurately predicted using the empirical formula of the line in Fig. 8.

Fig. 9 shows damage sensing of an actual hybrid part of an automobile sunroof using 2D-ER mapping. The 4-probe electrical contacts were formed on the surface of the specimen to measure ER of each section, and the evaluated ER were arranged to obtain the 2D mapping. The initial ERs of the parts were measured. The specimen was heated at 80 °C for 1 h in an oven. The specimen was cooled to 30 °C and ERs were measured to determine the ER difference. Generally, in non-damaged areas, the ER difference was changed a little bit. The decrease in ER occurred because of heat migration in the CFs which was activated by the latent heat energy of the CF/PA composite. However, the ER increased in the red circle in figure. The hybrid part of automobile sunroof was delaminated between steel and CF/PA composite by thermal shock and the thermal stress occurred at the interface mainly. The damage of real part of automobile could be sensed and monitored successfully using ER measurements and their 2D ER mapping *in-situ*.

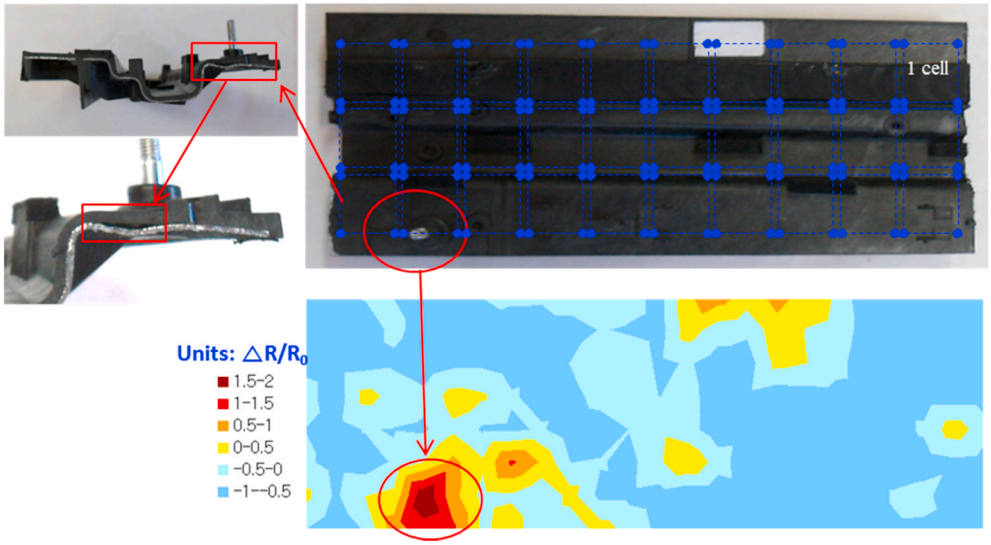

Fig. 9. Photos of actual CF/PA-metal hybrid sunroof part and its 2D mapping of verification of cracks in parts.

4. Conclusions

In this paper, the damage of CFRTC was sensed during tensile and flexural testing, using ER measurements and 2D ER mapping for CF/PA composites with different CF weight fractions. In the tensile test, the tensile load was measured while ER differences were used to evaluate the damage and CF dispersion. Tensile loading was studied using ER measurements and the trend of ER difference appeared to be consistent well with CF dispersion. However, in the flexural test, the load and damage of CFRTC were not matched exactly and further study could be needed for damage sensing in flexural tests. For the flexural tests, the accuracy of ER difference was lower than for the tensile test. The CF fraction in CFRTC was evaluated from the using the empirical equation of CF contents-ER. It exhibited accurate consistence at high CF contents over 20 wt%. However, the below 20 wt% CF fractions exhibited significant deviations probably due to poor CF dispersion. Both tensile and flexural stresses were correlated well with the fracture mechanisms of specimens and was proved successfully *in-situ*.

CRediT authorship contribution statement

Jong-Hyun Kim: Writing - original draft, Data curation, Writing - review & editing, Visualization, Formal analysis. **Pyeong-Su Shin:** Formal analysis, Visualization. **Dong-Jun Kwon:** Writing - original draft, Writing - review & editing, Data curation, Visualization, Conceptualization, Formal analysis. **Joung-Man Park:** Formal analysis, Writing - review & editing, Visualization, Supervision.

Declaration of competing interest

The authors declare that they have no known competing financial interests or personal relationships that could have appeared to influence the work reported in this paper.

Acknowledgements

This work was supported by National Research Foundation of Korea (NRF) grants funded by the Korea government (MOE) (No. 2016R1D1A1B01012620), 2016–2022; and Basic Science Research Program (No. 2020R1A6A1A0303869711), 2020–2023, respectively.

References

[1] T. Ishikawa, K. Amaoka, Y. Masubuchi, T. Yamamoto, A. Yamanaka, M. Arai, J. Takahashi, Overview of automotive structural composites technology developments in Japan, Compos. Sci. Technol. 115 (2018) 221–246.
[2] O.T. Adesina, T. Jamiru, E.R. Sadiku, O.F. Ogunbiyi, L.W. Beneke, Mechanical evaluation of hybrid natural fibre–reinforced polymeric composites for automotive bumper beam: a review, Int. J. Adv. Manuf. Technol. 103 (2019) 1781–1797.
[3] N. Haibin, L. Na, H. Ahmed Arabi, C. Krishan, S. Mohamed, P. Selvum, A review of Long fibre-reinforced thermoplastic or long fibre thermoplastic (LFT) composites, Int. Mater. Rev. 65 (2020) 164–188.
[4] G. Fernando, C. Constantin, Fracture toughness differences of injection molding long fiber reinforced thermoplastic, J. Reinf. Plast. Compos. 20 (2001) 810–820.
[5] H.S. Tan, Y.Z. Yu, L.P. Li, X.J. Liu, Z.X. Tan, Y.Y. Gong, A.X. Li, Mechanical properties of long glass fiber reinforced polyolefin composites, Polym. Plast. Technol. Eng. 54 (2015) 1343–1348.
[6] H.J. An, J.S. Kim, K.Y. Kim, D.Y. Lim, D.H. Kim, Mechanical and thermal properties of long carbon fiber-reinforced polyamide 6 composites, Fibers Polym. 15 (2014) 2355–2359.
[7] D. Teixeirea, M. Giovanela, L.B. Gonella, J.S. Crespo, Influence of flow restriction on the microstructure and mechanical properties of long glass fiber-reinforced polyamide 6.6 composites for automotive applications, Mater. Des. 47 (2013) 287–294.
[8] C. Ozklan, N. Gamze Karsli, A. Aytac, V. Deniz, Short carbon fiber reinforced polycarbonate composites: Effects of different sizing materials, Compos. B Eng. 62 (2014) 230–235.
[9] Y. Tan, X. Wang, D. Wu, Preparation, microstructures, and properties of long-glass-fiber-reinforced thermoplastic composites based on polycarbonate/poly(butylene terephthalate) alloys, J. Reinforc. Plast. Compos. 34 (2015) 1804–1820.
[10] C. Lohr, B. Beck, F. Henning, K. André Weidenmann, P. Elsner, Mechanical properties of foamed long glass fiber reinforced polyphenylene sulfide integral sandwich structures manufactured by direct thermoplastic foam injection molding, Compos. Struct. 220 (2019) 371–385.
[11] B. Vieille, A. Coppalle, M.A. Maaroufi, F. Barbe, Influence of matrix nature on the post-fire mechanical behaviour of notched polymer-based composite structures for high temperature applications, Compos. B Eng. 100 (2016) 114–124.
[12] M. Dkier, M. Yousfi, K. Lamnawar, A. Maazouz, Chemo-rheological studies and monitoring of high-Tg reactive polyphtalamides towards a fast innovative RTM processing of fiberreinforced thermoplastic composites, Eur. Polym. J. 120 (2019) 109227.
[13] C. Chen, C. Zhang, Z. Zhao, Y. Wang, S.C. Wong, Y. Li, Effect of fiber reinforcement and fabrication process on the dynamic flexural behavior of PEEK composites, Int. J. Mech. Sci. 155 (2019) 170–177. Y.
[14] Y. Masubuchi, M. Terada, A. Yamanaka, T. Yamamoto, T. Ishikawa, Distribution function of fiber length in thermoplastic composites, Compos. Sci. Technol. 134 (2016) 43–48.
[15] M.S. Asenjan, A.R. Sabet, M. Nekoomanesh, Long fiber thermoplastic composites under high-velocity impact: study of fiber length, J. Compos. Mater. 53 (2018) 1–8.
[16] D.J. Kwon, P.S. Shin, J.H. Kim, K.L. DeVries, J.M. Park, Evaluation of dispersion and damage sensing of carbon fiber/polypropylene (PP)-polyamide (PA) composites using 2 dimensional electrical resistance mapping, Compos. Appl. Sci. Manuf. 90 (2016) 417–423.
[17] H.S. Huan, Influence of phase shift on the responses of woven laminated composites, Compos. Struct. 130 (2015) 143–154.

[18] Y. Song, U. Gandhi, A. Koziel, S. Vallury, A. Yang, Effect of the initial fiber alignment on the mechanical properties for GMT composite materials, J. Thermoplast. Compos. Mater. 31 (2018) 91–109.
[19] J.B. Kim, M.G. Jeong, H. Böhm, J. Richter, N. Modler, Experimental investigation into static and dynamic axial crush of composite tubes of glass-fiber mat/PA6 laminates, Compos. B Eng. 181 (2020) 107590.
[20] M. Golzar, H. Brünig, E. Mäder, Commingled hybrid yarn diameter ratio in continuous fiber-reinforced thermoplastic composites, J. Thermoplast. Compos. Mater. 20 (2007) 17–26.
[21] G. Guo, C. Kethineni, Direct injection molding of hybrid polypropylene/wood-fiber composites reinforced with glass fiber and carbon, fiber 106 (2020) 201–209.
[22] J.M.M. Anderson, A.D. Jackson, H.G. Martin, J.G. Schubert, Nondestructive evaluation of naval munitions using X-ray CT, Res. Nondestr. Eval. 22 (2011) 16–30.
[23] J. Wang, J. Zhang, T. Chang, H.L. Cui, A comparative study of non-destructive evaluation of glass fiber reinforced polymer composites using terahertz, X-ray, and ultrasound imaging, Int. J. Precis. Eng. Manuf. 20 (2019) 963–972.
[24] J.H. Kim, D.J. Kwon, P.S. Shin, Y.M. Baek, H.S. Park, K.L. DeVries, J.M. Park, New evaluation of interfacial properties and damage sensing in CFRC by VARTM using 3D ER mapping, Compos. B Eng. 155 (2018) 178–186.
[25] A. Esmaeili, C. Sharufatti, D. Ma, A. Manes, A. Jimenez-Suarez, A. Urena, D. Dellasega, A.M.S. Hamouda, Strain and crack growth sensing capability of SWCNT reinforced epoxy in tensile and mode I fracture tests, Compos. Sci. Technol. 186 (2020) 107918.
[26] A.S. Wu, W.J. Na, W.R. Yu, J.H. Byun, T.W. Chou, Carbon nanotube film interlayer for strain and damage sensing in composites during dynamic compressive loading, Appl. Phys. Lett. 101 (2012) 221909.